ATLAS PUB Note

ATL-PHYS-PUB-2023-027

22nd September 2023

Top EFT summary plots September 2023

The ATLAS and CMS Collaborations

This note presents figures that summarise the limits on effective field theory (EFT) operators derived from measurements of the ATLAS top working group and LHC Top working group (ATLAS+CMS). Measurements of top quark pair production, single top production and associated production processes are interpreted within the SMEFT framework. FCNC processes are also included. Individual bounds on Wilson coefficients are derived at the 68% and 95% CL.

The Standard Model of Particle Physics (SM) has proven to be a succesful theory both in describing observed phenomena as well as making predictions which have later been confirmed by experiments. However, there remain unanswered questions that the SM fails to answer such as the asymmetry between matter and anti-matter, the hierarchy between the Planck mass scale and the electroweak scale set by the vacuum expectation value of the Higgs field or the nature of the dark matter and dark energy present in our Universe. This makes mandatory the searches for new physics at the LHC. New physics can be probed directly by searching for new states. However, if the mass of such particles lies outside the direct reach at LHC energies, it is still possible to infer their existence by indirect means.

The Effective Field Theory (EFT) [1] provides a model-independent framework for such indirect searches. Within this framework, the SM is regarded as a low-energy approximation of a more fundamental theory involving interactions at an energy scale Λ. New physics is then parametrised in terms of higher dimension operators which only include SM fields. The effective Lagrangian then becomes

$$\mathcal{L}_{\text{Eff}} = \mathcal{L}_{\text{SM}} + \sum_{d,i} \frac{c_i^{(d)}}{\Lambda^{d-4}} O_i^{(d)}, \tag{1}$$

where $\mathcal{L}_{\text{SM}}$ is the SM Lagrangian, $O_i^{(d)}$ are the effective operators of dimension d and the complex coefficients $c_i^{(d)}$ are the Wilson coefficients that parameterise the strength of the interaction.

The measurements included in these summary figures use the Warsaw basis [2] as recommended by the LHC Top Working Group [3]. For all measurements the series is truncated at dimension-6 and the value $\Lambda = 1$ TeV is used.

The bounds in ATLAS-only plots are reported taking into account only the linear term of the SMEFT operator (red lines) and/or the linear and the quadratic terms (blue line), except for Figure 3, where only the quadratic term is reported. The dashed line represents the 95% CL limits while the solid one accounts for the 68% CL limits. Limits on each individual operator are derived fixing the rest to the SM value, except for $C_{\text{tW}}^{[I]}$ and C_{tW} coefficients, which are fitted simultaneously from the single top polarisation measurement.

Figure 1 shows the derived bounds on two-quark operators obtained from ATLAS measurements only. The measurements include:

- ATLAS, Single top t-channel, top polarization [4]
- ATLAS, $t\bar{t}Z$ [5]
- ATLAS, $t\bar{t}$ l+jets boosted [6]
- ATLAS, $t\bar{t}$ rapidity asymmetry [7]

Figure 2 shows the derived bounds on four-quark operators obtained from ATLAS measurements only. In this plot, all other operators are fixed to zero (their SM expectation). The measurements include:

- ATLAS, $t\bar{t}$ l+jets boosted [6]
- ATLAS, $t\bar{t}$ all-hadronic boosted [8]
- ATLAS, $t\bar{t}$ rapidity asymmetry [7]
- ATLAS, $t\bar{t}$ +jet energy asymmetry [9]

Figure 3 shows the derived bounds on dimension-6 FCNC EFT operators in vertical formats. In this plot, all other operators are fixed to zero (their SM expectation). The measurements included:

- ATLAS, FCNC tqZ [10]

- ATLAS, FCNC tqH [11]

- ATLAS, FCNC tqg [12]

- ATLAS, FCNC $tq\gamma$ [13]

Figures 4 and 5 show the derived bounds on dimension-6 top quark EFT operators (excluding FCNCs) in vertical and horizontal formats respectively. In these plots, all other operators are fixed to zero (their SM expectation). The measurements include:

- CMS, $t\bar{t}$ dilepton [14]

- ATLAS, $t\bar{t}Z$ [5]

- CMS, $t\bar{t}$ spin correlations [15]

- CMS, 4 top quarks [16]

- CMS, $t\bar{t}$ and tW, BSM search [17]

- CMS, $t\bar{t}Z$ [18]

- ATLAS+CMS, W helicity [19]

- CMS, $t\bar{t} + Z/W/H$, tZq, tHq [20]

- CMS, $tZq/t\bar{t}Z$ [21]

- ATLAS, Single top t-channel, top polarization [4]

- ATLAS, $t\bar{t}$ l+jets boosted [6]

- ATLAS, $t\bar{t}$ +jet energy asymmetry [9]

- ATLAS, $t\bar{t}$ all-hadronic boosted [8]

- CMS, $t\bar{t}\gamma$ [22]

- ATLAS, $t\bar{t}$ rapidity asymmetry [7]

- CMS, $t\bar{t}$+boosted Z/H [23]

- CMS, $t\bar{t}H$, $t\bar{t}\ell\nu$, $t\bar{t}\ell\ell$, $t\ell\ell q$, tHq, $t\bar{t}t\bar{t}$ [24]

Figures 6 and 7 show the derived bounds on dimension-6 top quark EFT operators (excluding FCNCs) in vertical and horizontal formats respectively. In these plots, all other operators are profiled. The measurements include:

- CMS, 4 top quarks [16]

- CMS, $t\bar{t} + Z/W/H$, tZq, tHq [20]

- CMS, $tZq/t\bar{t}Z$ [21]

- ATLAS, Single top t-channel, top polarization [4]

- ATLAS, $t\bar{t}$ l+jets boosted [6]

- CMS, $t\bar{t}\gamma$ [22]

- CMS, $t\bar{t}$+boosted Z/H [23]

- CMS, $t\bar{t}H$, $t\bar{t}\ell\nu$, $t\bar{t}\ell\ell$, $t\ell\ell q$, tHq, $t\bar{t}t\bar{t}$ [24]

Figure 8 shows the derived bounds on dimension-6 FCNC EFT operators in vertical formats. In this plot, all other operators are fixed to zero (their SM expectation). The measurements include:

- CMS, $t\bar{t}$ and tW, BSM search [17]

- ATLAS, FCNC tqZ [10]

- ATLAS, FCNC tqH [11]

- ATLAS, FCNC tqg [12]

- ATLAS, FCNC $tq\gamma$ [13]

Figures 9 and 10 show the derived bounds on dimension-6 operators related to interactions with scalar bosons (excluding FCNCs). In these plots, all other operators are fixed to zero (their SM expectation). The measurements include:

- ATLAS, $t\bar{t}Z$ [5]

- CMS, $t\bar{t}$ and tW, BSM search [17]

- CMS, $t\bar{t}Z$ [18]

- CMS, $t\bar{t} + Z/W/H$, tZq, tHq [20]

- CMS, $tZq/t\bar{t}Z$ [21]

- CMS, $t\bar{t}$+boosted Z/H [23]

- CMS, $t\bar{t}H$, $t\bar{t}\ell\nu$, $t\bar{t}\ell\ell$, $t\ell\ell q$, tHq, $t\bar{t}t\bar{t}$ [24]

Figures 11 and 12 show the derived bounds on dimension-6 operators related to interactions with vector bosons (excluding FCNCs). In these plots, all other operators are fixed to zero (their SM expectation). The measurements include:

- CMS, $t\bar{t}$ dilepton [14]

- ATLAS, $t\bar{t}Z$ [5]

- CMS, $t\bar{t}$ spin correlations [15]

- CMS, $t\bar{t}$ and tW, BSM search [17]

- CMS, $t\bar{t}Z$ [18]

- ATLAS+CMS, W helicity [19]

- CMS, $t\bar{t} + Z/W/H$, tZq, tHq [20]

- CMS, $tZq/t\bar{t}Z$ [21]

- ATLAS, Single top t-channel, top polarization [4]

- ATLAS, $t\bar{t}$ l+jets boosted [6]

- CMS, $t\bar{t}\gamma$ [22]

- ATLAS, $t\bar{t}$ rapidity asymmetry [7]

- CMS, $t\bar{t}$+boosted Z/H [23]

- CMS, $t\bar{t}H$, $t\bar{t}\ell\nu$, $t\bar{t}\ell\ell$, $t\ell\ell q$, tHq, $t\bar{t}t\bar{t}$ [24]

Figures 13 and 14 show the derived bounds on dimension-6 operators related to interactions with vector bosons (excluding FCNCs). In these plots, all other operators are profiled. The measurements include:

- CMS, $t\bar{t} + Z/W/H$, tZq, tHq [20]

- CMS, $tZq/t\bar{t}Z$ [21]

- ATLAS, Single top t-channel, top polarization [4]

- ATLAS, $t\bar{t}$ l+jets boosted [6]

- CMS, $t\bar{t}\gamma$ [22]

- CMS, $t\bar{t}$+boosted Z/H [23]

- CMS, $t\bar{t}H$, $t\bar{t}\ell\nu$, $t\bar{t}\ell\ell$, $t\ell\ell q$, tHq, $t\bar{t}t\bar{t}$ [24]

Figures 15 and 16 show the derived bounds on dimension-6 operators related to four-fermion interactions (excluding FCNCs). In these plots, all other operators are fixed to zero (their SM expectation). The measurements include:

- CMS, 4 top quarks [16]

- CMS, $t\bar{t} + Z/W/H$, tZq, tHq [20]

- ATLAS, $t\bar{t}$ l+jets boosted [6]

- ATLAS, $t\bar{t}$ +jet energy asymmetry [9]

- ATLAS, $t\bar{t}$ all-hadronic boosted [8]

- ATLAS, $t\bar{t}$ rapidity asymmetry [7]

- CMS, $t\bar{t}H$, $t\bar{t}\ell\nu$, $t\bar{t}\ell\ell$, $t\ell\ell q$, tHq, $t\bar{t}t\bar{t}$ [24]

Figures 17 and 18 show the derived bounds on dimension-6 operators related to four-fermion interactions (excluding FCNCs). In these plots, all other operators are fixed to zero (their SM expectation). The measurements include:

- CMS, 4 top quarks [16]

- CMS, $t\bar{t} + Z/W/H$, tZq, tHq [20]

- ATLAS, $t\bar{t}$ l+jets boosted [6]

- CMS, $t\bar{t}H$, $t\bar{t}\ell\nu$, $t\bar{t}\ell\ell$, $t\ell\ell q$, tHq, $t\bar{t}t\bar{t}$ [24]
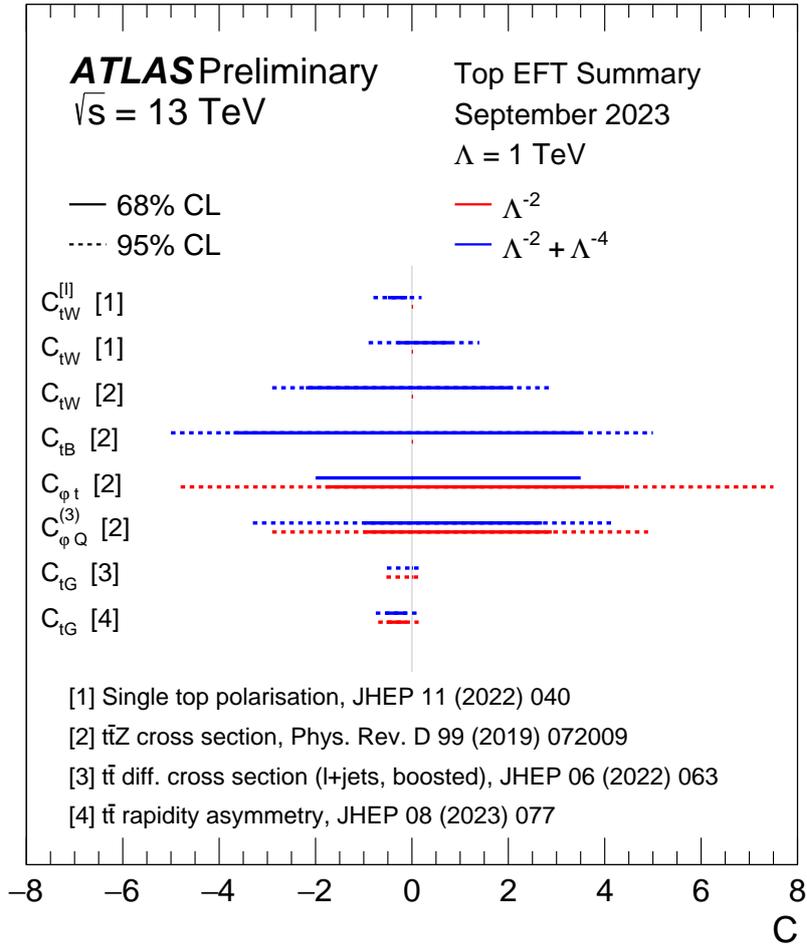
Figure 1: Summary of constraints on two-fermion SMEFT operators from top-quark measurements at the ATLAS experiment. The bounds on the Wilson coefficients are reported at the 68% CL (solid) and/or 95% CL (dashed) depending on the availability in the corresponding measurement. The bounds are reported without (red) and/or with (blue) taking into account the quadratic term of the SMEFT operator, depending on the availability in the corresponding measurement. Limits on each individual operator are derived fixing the rest to the SM value (except for $C_{tW}^{[I]}$ and C_{tW} coefficients, which are fitted simultaneously from the single top polarisation measurement). Interpretations use the SMEFT framework and the Warsaw basis. The vertical bar represents the SM prediction.
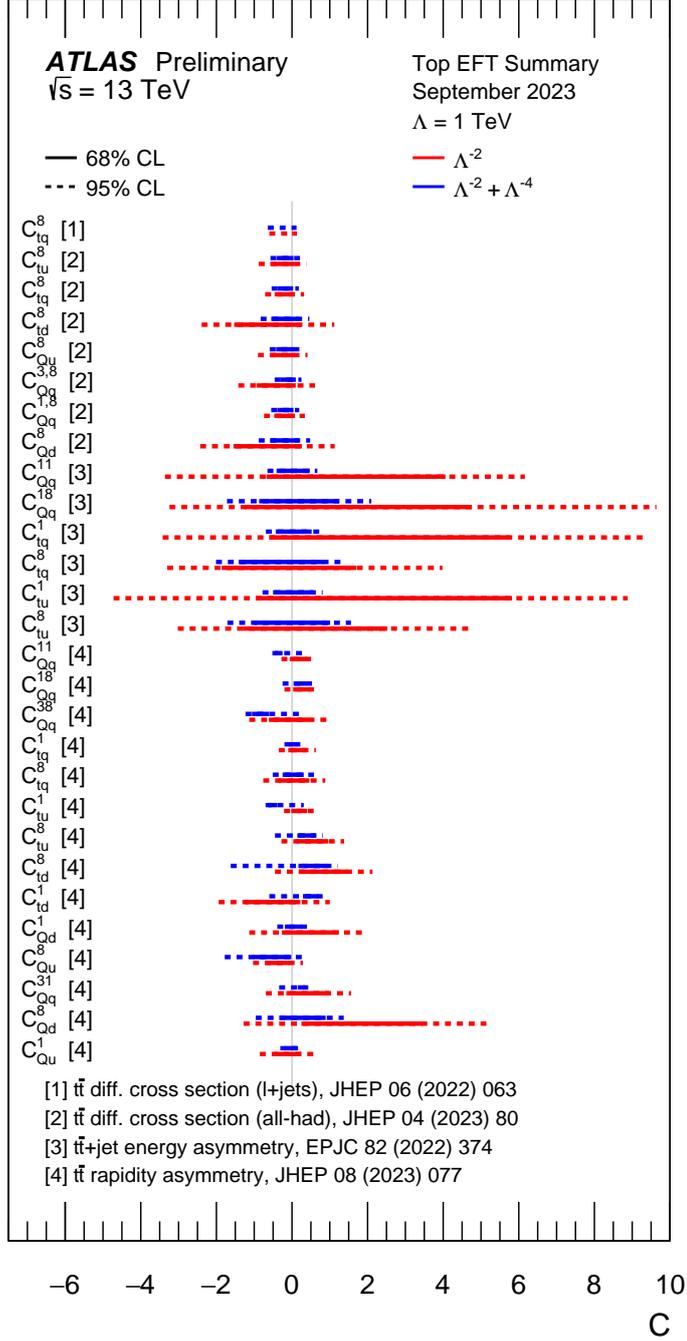
Figure 2: Summary of constraints on four-fermion SMEFT operators from top-quark measurements at the ATLAS experiment. The bounds on the Wilson coefficients are reported at the 68% CL (solid) and/or 95% CL (dashed) depending on the availability in the corresponding measurement. The bounds are reported without (red) and/or with (blue) taking into account the quadratic term of the SMEFT operator, depending on the availability in the corresponding measurement. Limits on each individual operator are derived fixing the rest to the SM value. Interpretations use the SMEFT framework and the Warsaw basis. The vertical bar represents the SM prediction. Only the most stringent limit from Ref. [7] is quoted.
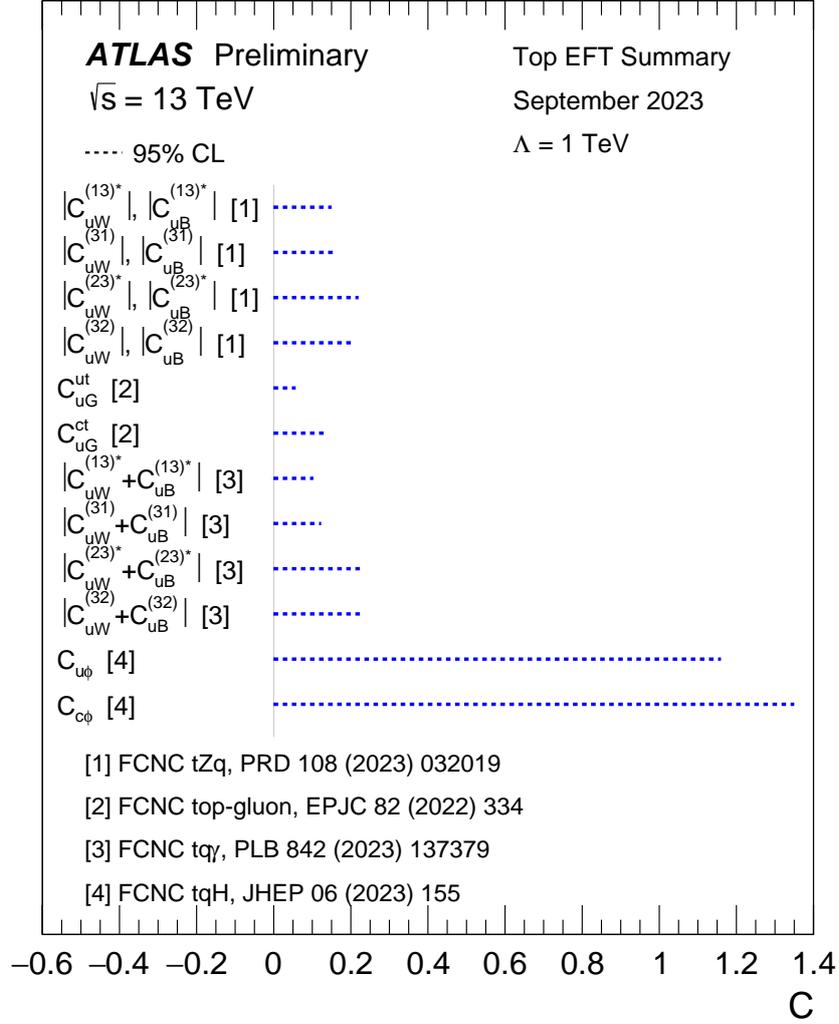
Figure 3: Summary of constraints on FCNC SMEFT operators from top-quark measurements at the ATLAS experiment. The bounds on the Wilson coefficients are reported at the 95% CL. The quadratic term of the SMEFT operator is taken into account for the interpretation (the linear term is negligible). Limits on each individual operator are derived fixing the rest to the SM value. Interpretations use the SMEFT framework and the Warsaw basis. The vertical bar represents the SM prediction.
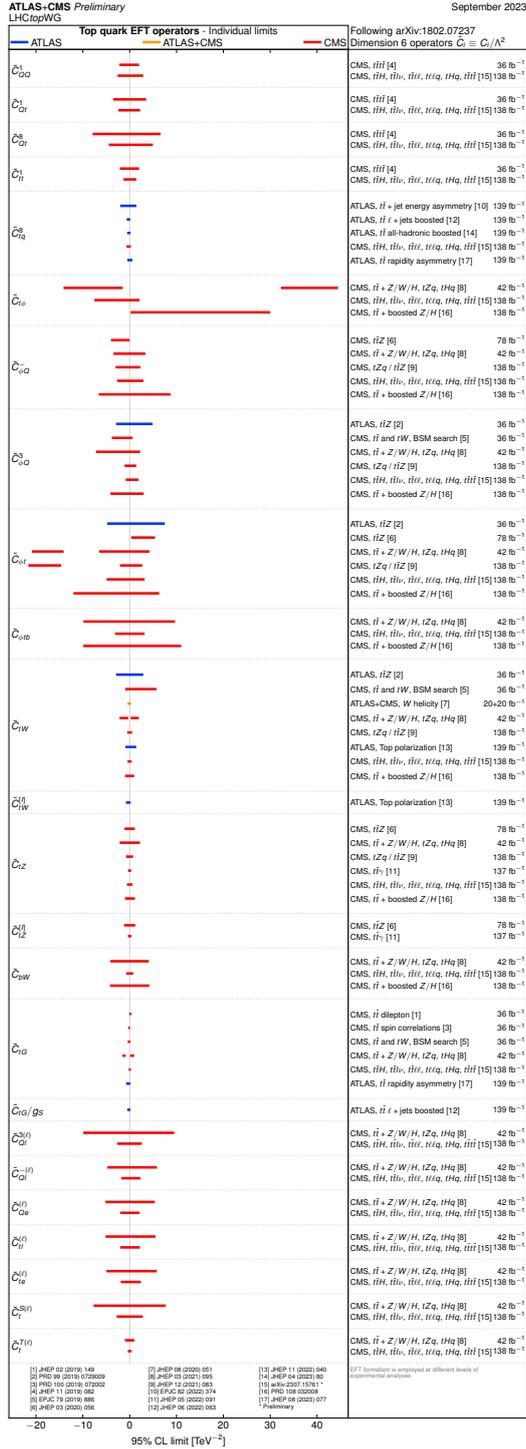
Figure 4: Summary of the 95% confidence level observed limits on the effective field theory Wilson coefficients of the dimension-6 operators related to interactions involving top quarks, as obtained by the ATLAS and CMS Collaborations. The results are reported as individual constraints assuming new physics contributions from one specific operator at a time. Interpretations use the SMEFT framework and the Warsaw basis. The formalism is employed at different levels of the experimental analyses, from the interpretation of measured observables to a comparison of the data to simulations at the detector level. Most interpretations follow the LHCtopWG recommendations from arXiv:1802.07237. In JHEP 06 (2022) 063, the limit is derived for the coefficient c_{tG} normalised with the strong coupling, g_S, as implemented in SMEFT@NLO. Vertical format.
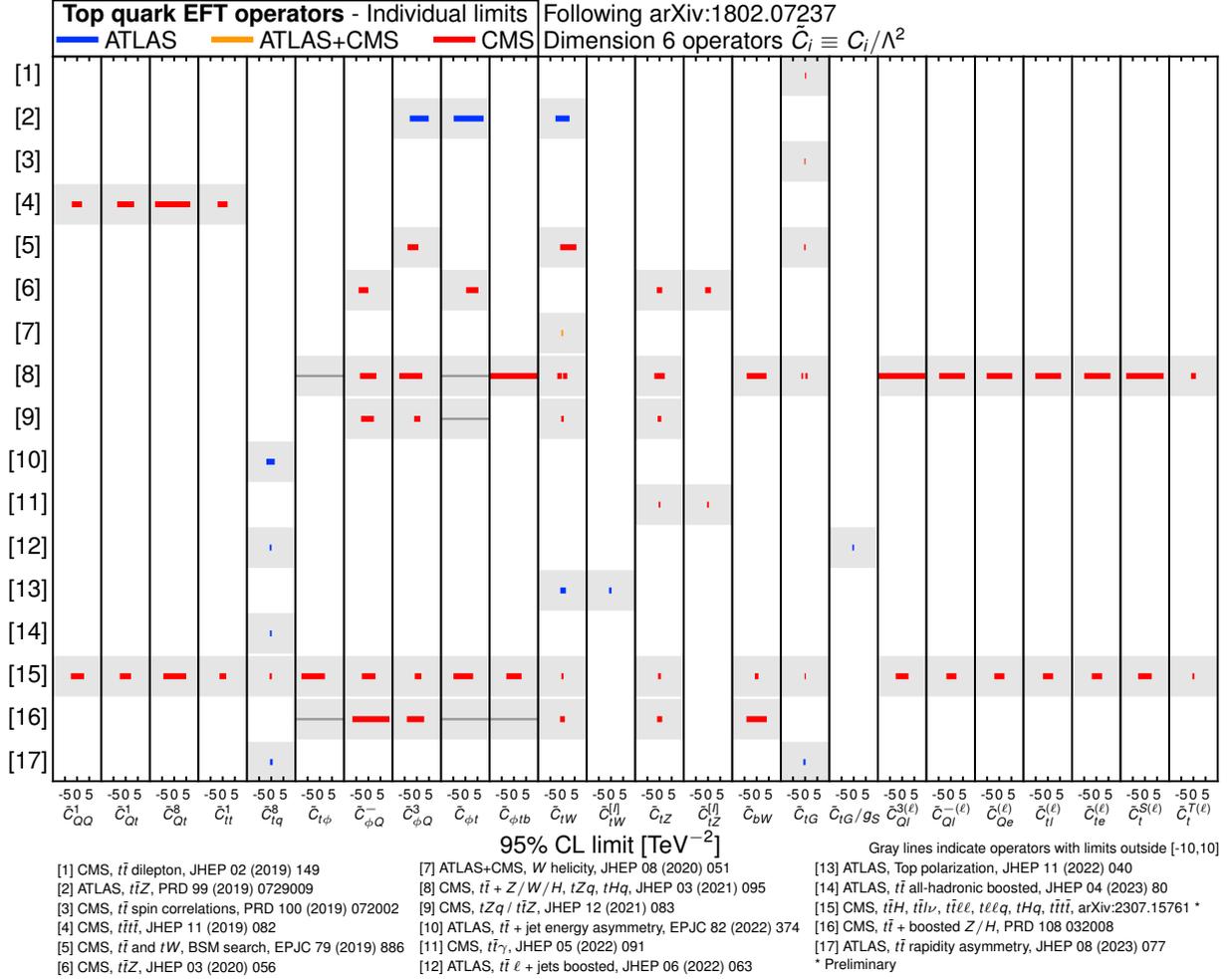
Figure 5: Summary of the 95% confidence level observed limits on the effective field theory Wilson coefficients of the dimension-6 operators related to interactions involving top quarks, as obtained by the ATLAS and CMS Collaborations. The results are reported as individual constraints assuming new physics contributions from one specific operator at a time. Interpretations use the SMEFT framework and the Warsaw basis. The formalism is employed at different levels of the experimental analyses, from the interpretation of measured observables to a comparison of the data to simulations at the detector level. Most interpretations follow the LHCtopWG recommendations from arXiv:1802.07237. In JHEP 06 (2022) 063, the limit is derived for the coefficient c_{tG} normalised with the strong coupling, g_S, as implemented in SMEFT@NLO. Horizontal format.
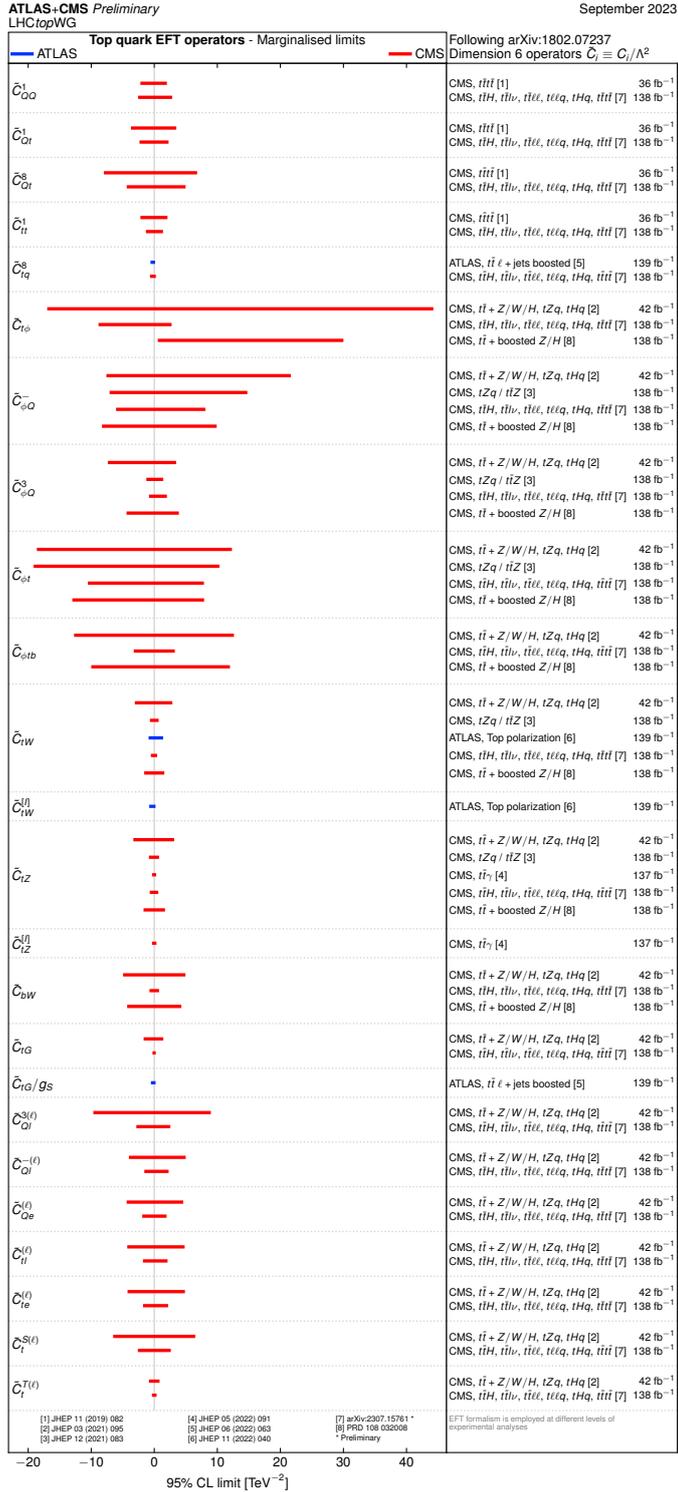
Figure 6: Summary of the 95% confidence level observed limits on the effective field theory Wilson coefficients of the dimension-6 operators related to interactions involving top quarks, as obtained by the ATLAS and CMS Collaborations. The results are reported as marginalised constraints, treating all Wilson coefficients contributing to a given process as free parameters. The effect of a given Wilson coefficient is considered in multiple processes, where indicated in the references, and across multiple bins of differential measurements. Each row presents all the marginalised constraints obtained from a single fit. In JHEP 06 (2022) 063, the limit is derived for the coefficient c_{tG} normalised with the strong coupling, g_S, as implemented in SMEFT@NLO. Vertical format.
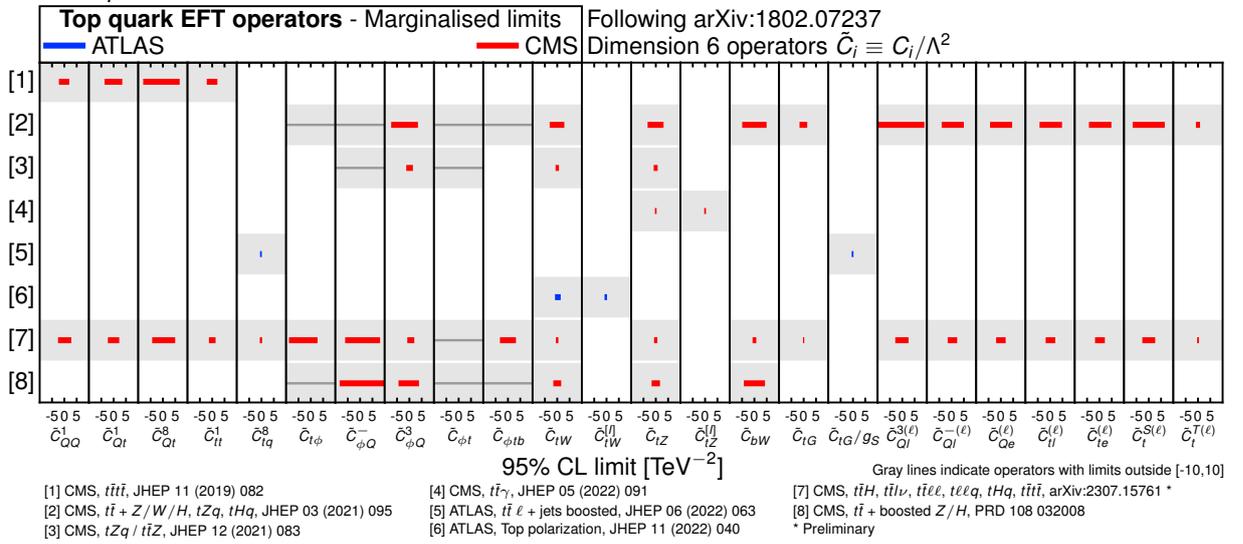
Figure 7: Summary of the 95% confidence level observed limits on the effective field theory Wilson coefficients of the dimension-6 operators related to interactions involving top quarks, as obtained by the ATLAS and CMS Collaborations. The results are reported as marginalised constraints, treating all Wilson coefficients contributing to a given process as free parameters. The effect of a given Wilson coefficient is considered in multiple processes, where indicated in the references, and across multiple bins of differential measurements. Each row presents all the marginalised constraints obtained from a single fit. In JHEP 06 (2022) 063, the limit is derived for the coefficient c_{tG} normalised with the strong coupling, g_S, as implemented in SMEFT@NLO. Horizontal format.
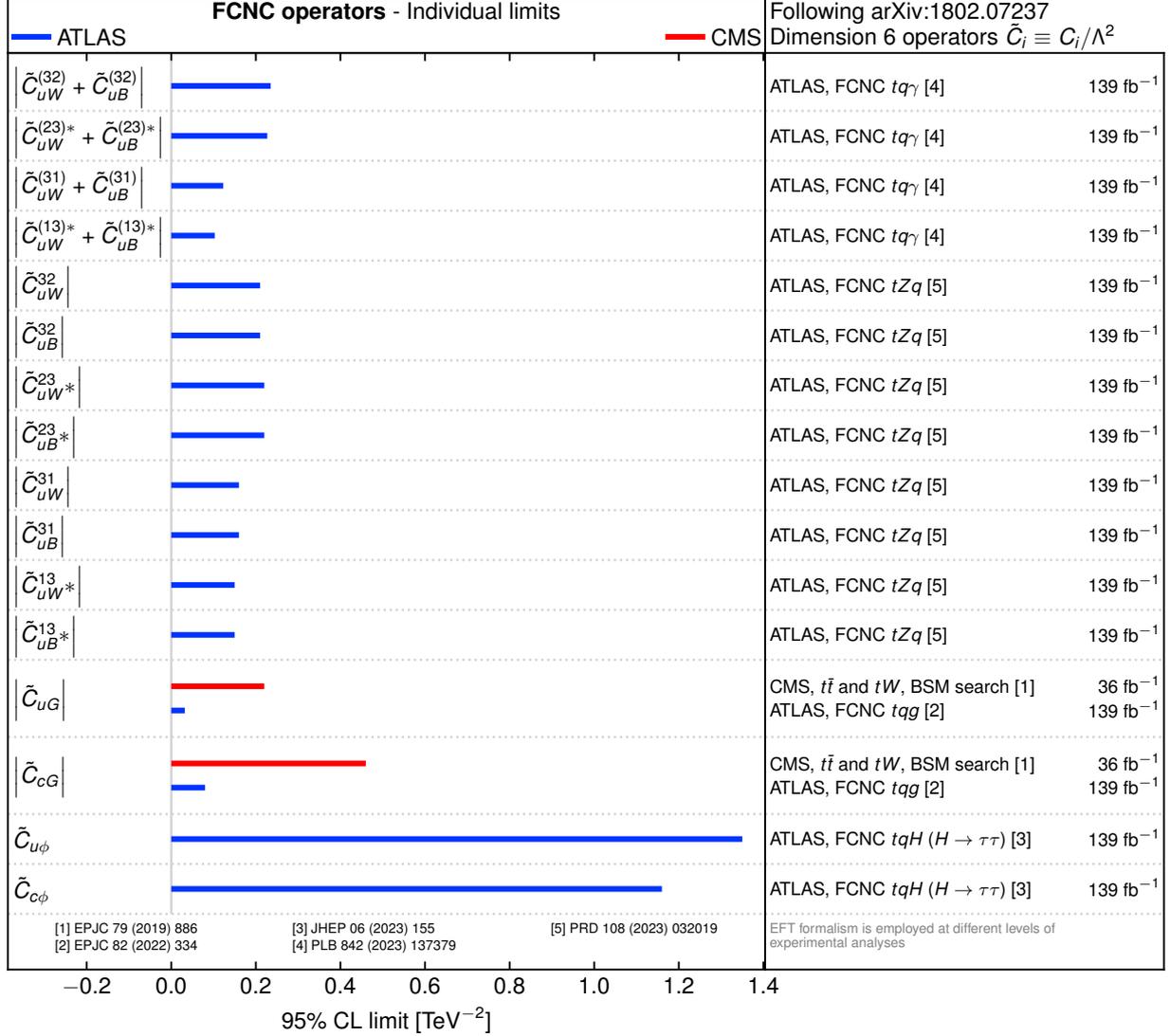
Figure 8: Summary of constraints on FCNC SMEFT operators from top-quark measurements, as obtained by the ATLAS and CMS Collaborations. The results are reported as individual constraints assuming new physics contributions from one specific operator at a time. Interpretations use the SMEFT framework and the Warsaw basis. The formalism is employed at different levels of the experimental analyses, from the interpretation of measured observables to a comparison of the data to simulations at the detector level. Most interpretations follow the LHCtopWG recommendations from arXiv:1802.07237. The definitions of operators O_{uG} and O_{cG} are different in the two searches from references EPJC 82 (2022) 334 and EPJC 79 (2019) 886. For comparison purposes in this plot, the limits for coefficients C_{uG} and C_{cG} from Ref. arXiv:2112.01302 are multiplied by factor $g_S(m_{\text{top}}^2)/2 = 0.57$ to be compatible with the definition used in Ref. EPJC 79 (2019) 886 as it is recommended in Ref. arXiv:1802.07237. Vertical format.
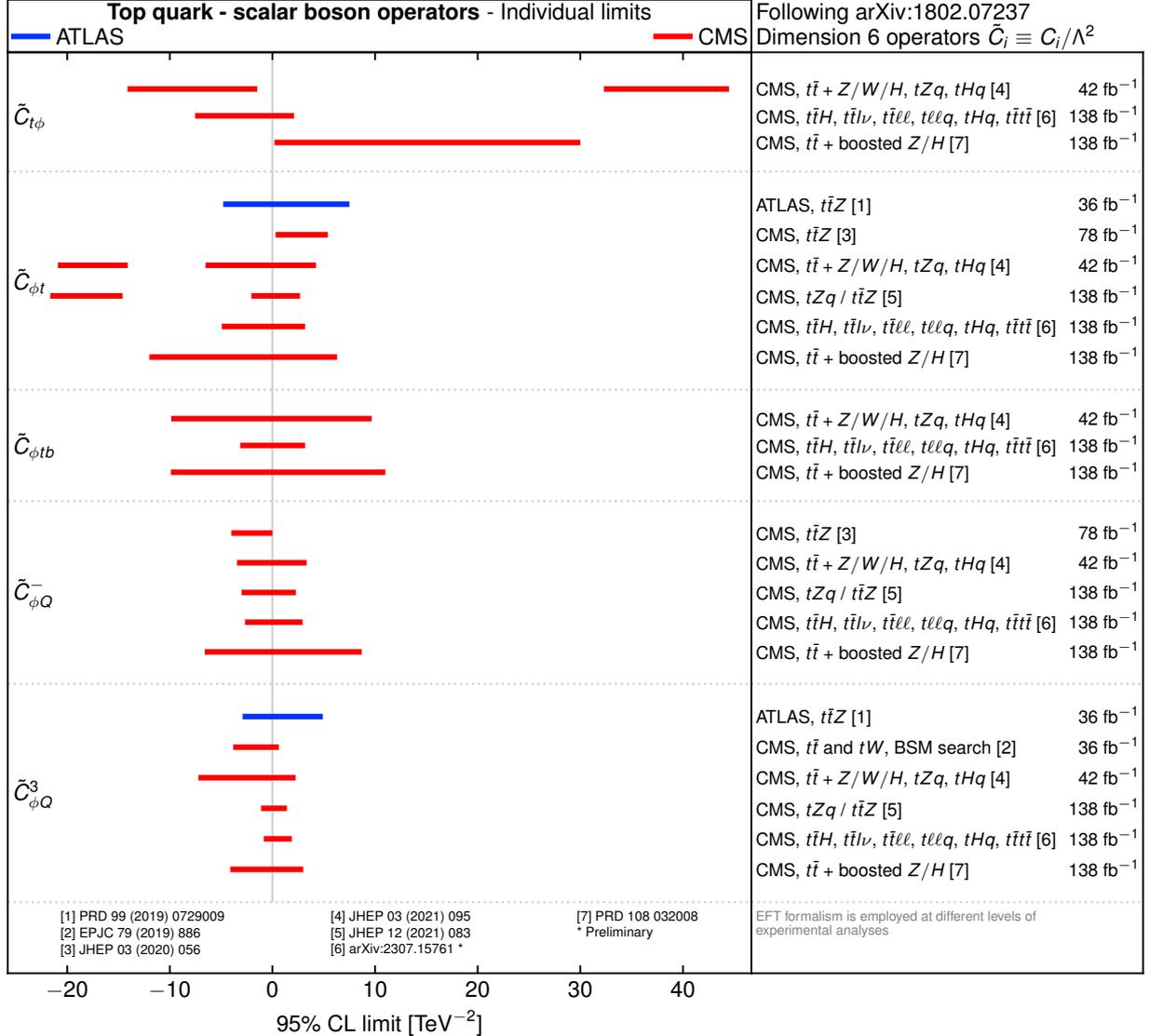
Figure 9: Summary of the 95% confidence level observed limits on the effective field theory Wilson coefficients of the dimension-6 operators related to (top) quark interaction with scalar bosons, as obtained by the ATLAS and CMS Collaborations. The results are reported as individual constraints assuming new physics contributions from one specific operator at a time. Interpretations use the SMEFT framework and the Warsaw basis. The formalism is employed at different levels of the experimental analyses, from the interpretation of measured observables to a comparison of the data to simulations at the detector level. Most interpretations follow the LHCtopWG recommendations from arXiv:1802.07237. Vertical format.

Figure 10: Summary of the 95% confidence level observed limits on the effective field theory Wilson coefficients of the dimension-6 operators related to (top) quark interaction with scalar bosons, as obtained by the ATLAS and CMS Collaborations. The results are reported as individual constraints assuming new physics contributions from one specific operator at a time. Interpretations use the SMEFT framework and the Warsaw basis. The formalism is employed at different levels of the experimental analyses, from the interpretation of measured observables to a comparison of the data to simulations at the detector level. Most interpretations follow the LHCtopWG recommendations from arXiv:1802.07237. Horizontal format.
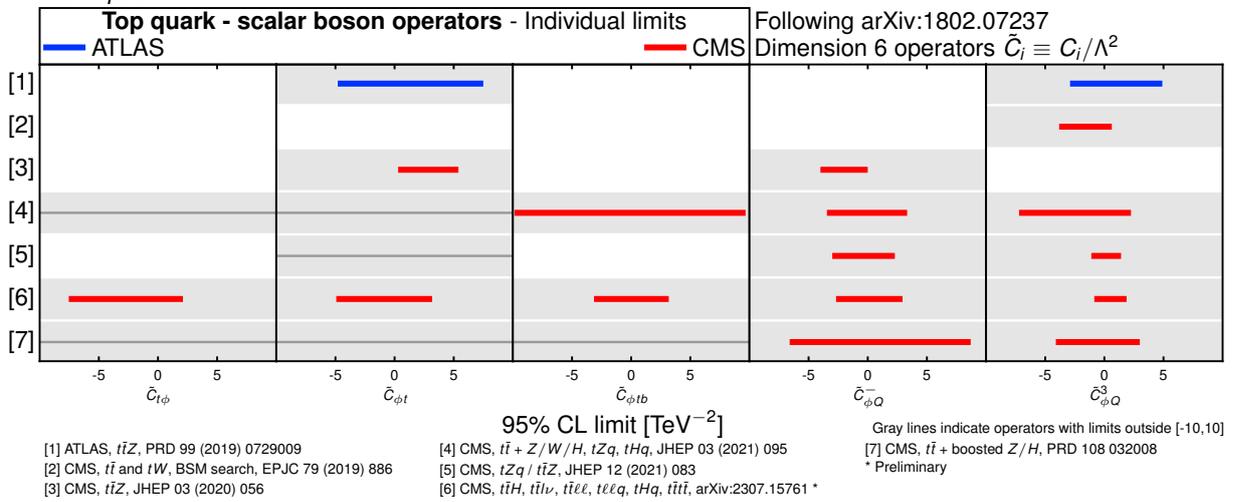
Figure 11: Summary of the 95% confidence level observed limits on the effective field theory Wilson coefficients of the dimension-6 operators related to (top) quark interaction with vector bosons, as obtained by the ATLAS and CMS Collaborations. The results are reported as individual constraints assuming new physics contributions from one specific operator at a time. Interpretations use the SMEFT framework and the Warsaw basis. The formalism is employed at different levels of the experimental analyses, from the interpretation of measured observables to a comparison of the data to simulations at the detector level. Most interpretations follow the LHCtopWG recommendations from arXiv:1802.07237. Vertical format.

(Top) quark - vector boson operators - Individual limits | Following arXiv:1802.07237

ATLAS — ATLAS+CMS — CMS | Dimension 6 operators $\tilde{C}_i \equiv C_i/\Lambda^2$

95% CL limit [TeV^{-2}]

$\tilde{C}_{tZ}$ $\tilde{C}_{tZ}^{[I]}$ $\tilde{C}_{tB}$ $\tilde{C}_{tW}$ $\tilde{C}_{tW}^{[I]}$ $\tilde{C}_{bW}$ $\tilde{C}_{tG}/g_S$ $\tilde{C}_{tG}$ $\tilde{C}_{tG}^{[I]}$

[1] CMS, $t\bar{t}$ dilepton, JHEP 02 (2019) 149
[2] ATLAS, $t\bar{t}Z$, PRD 99 (2019) 0729009
[3] CMS, $t\bar{t}$ spin correlations, PRD 100 (2019) 072002
[4] CMS, $t\bar{t}$ and tW, BSM search, EPJC 79 (2019) 886
[5] CMS, $t\bar{t}Z$, JHEP 03 (2020) 056

[6] ATLAS+CMS, W helicity, JHEP 08 (2020) 051
[7] CMS, $t\bar{t} + Z/W/H$, tZq, tHq, JHEP 03 (2021) 095
[8] CMS, $tZq / t\bar{t}Z$, JHEP 12 (2021) 083
[9] CMS, $t\bar{t}\gamma$, JHEP 05 (2022) 091
[10] ATLAS, $t\bar{t}\,\ell$ + jets boosted, JHEP 06 (2022) 063

[11] ATLAS, Top polarization, JHEP 11 (2022) 040
[12] CMS, $t\bar{t}H$, $t\bar{t}l\nu$, $t\bar{t}\ell\ell$, $t\ell\ell q$, tHq, $t\bar{t}t\bar{t}$, arXiv:2307.15761 *
[13] CMS, $t\bar{t}$ + boosted Z/H, PRD 108 032008
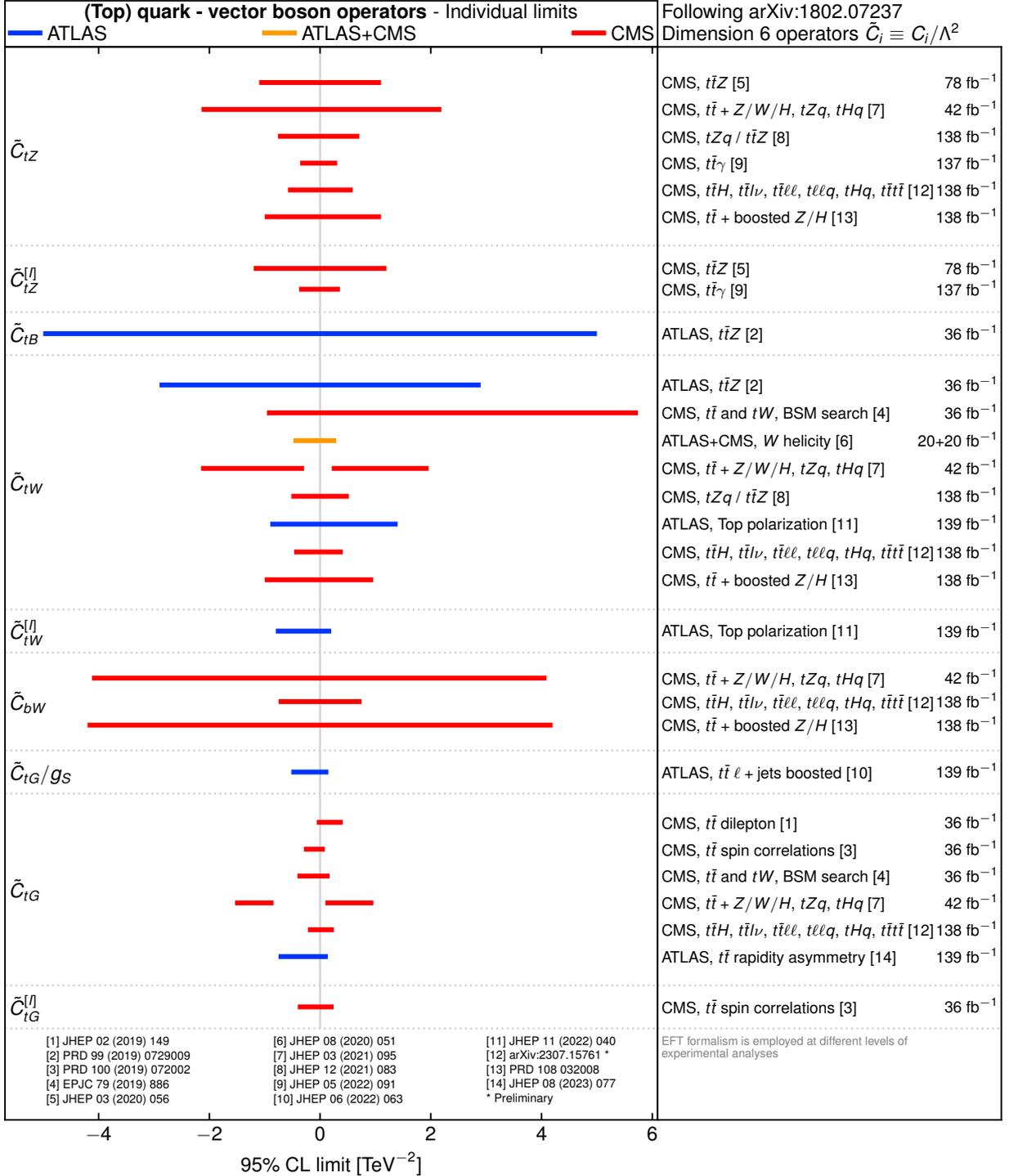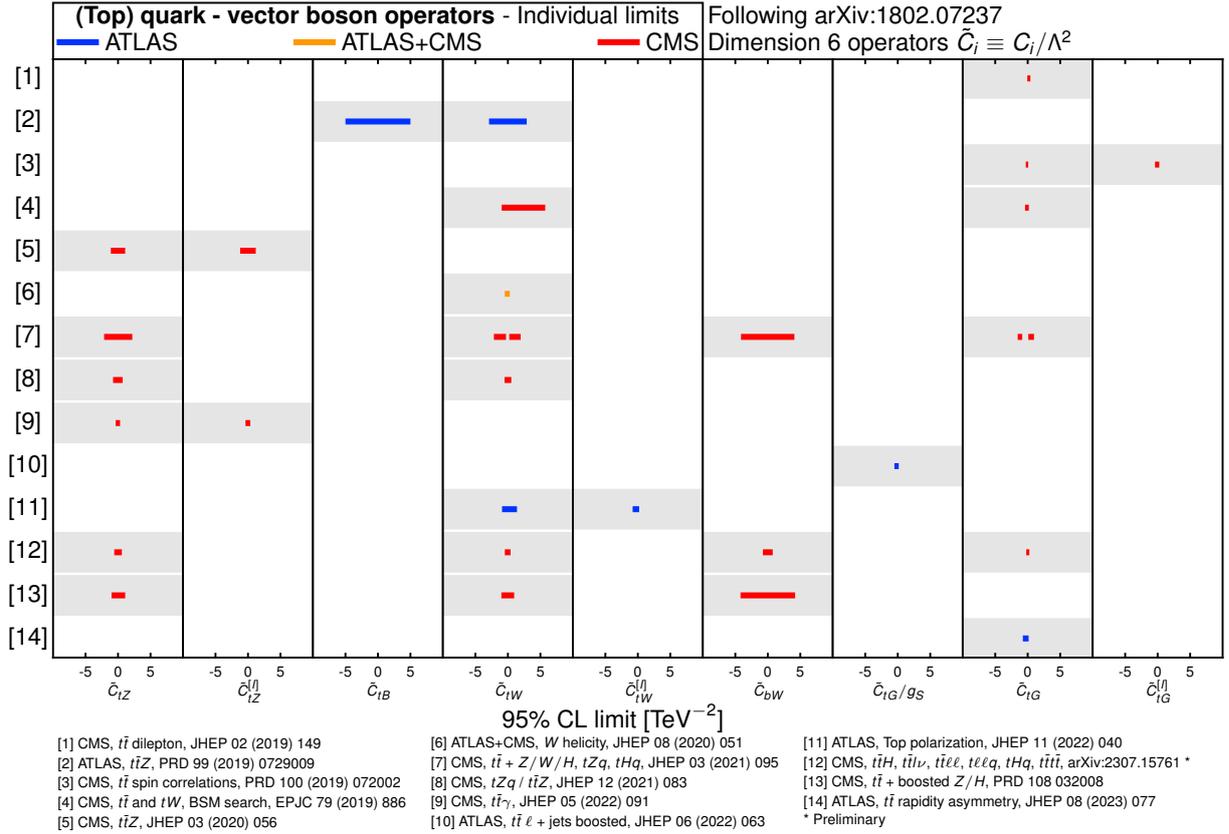[14] ATLAS, $t\bar{t}$ rapidity asymmetry, JHEP 08 (2023) 077
* Preliminary

Figure 12: Summary of the 95% confidence level observed limits on the effective field theory Wilson coefficients of the dimension-6 operators related to (top) quark interaction with vector bosons, as obtained by the ATLAS and CMS Collaborations. The results are reported as marginalised constraints, treating all Wilson coefficients contributing to a given process as free parameters. The effect of a given Wilson coefficient is considered in multiple processes, where indicated in the references, and across multiple bins of differential measurements. Each row presents all the marginalised constraints obtained from a single fit. Horizontal format.
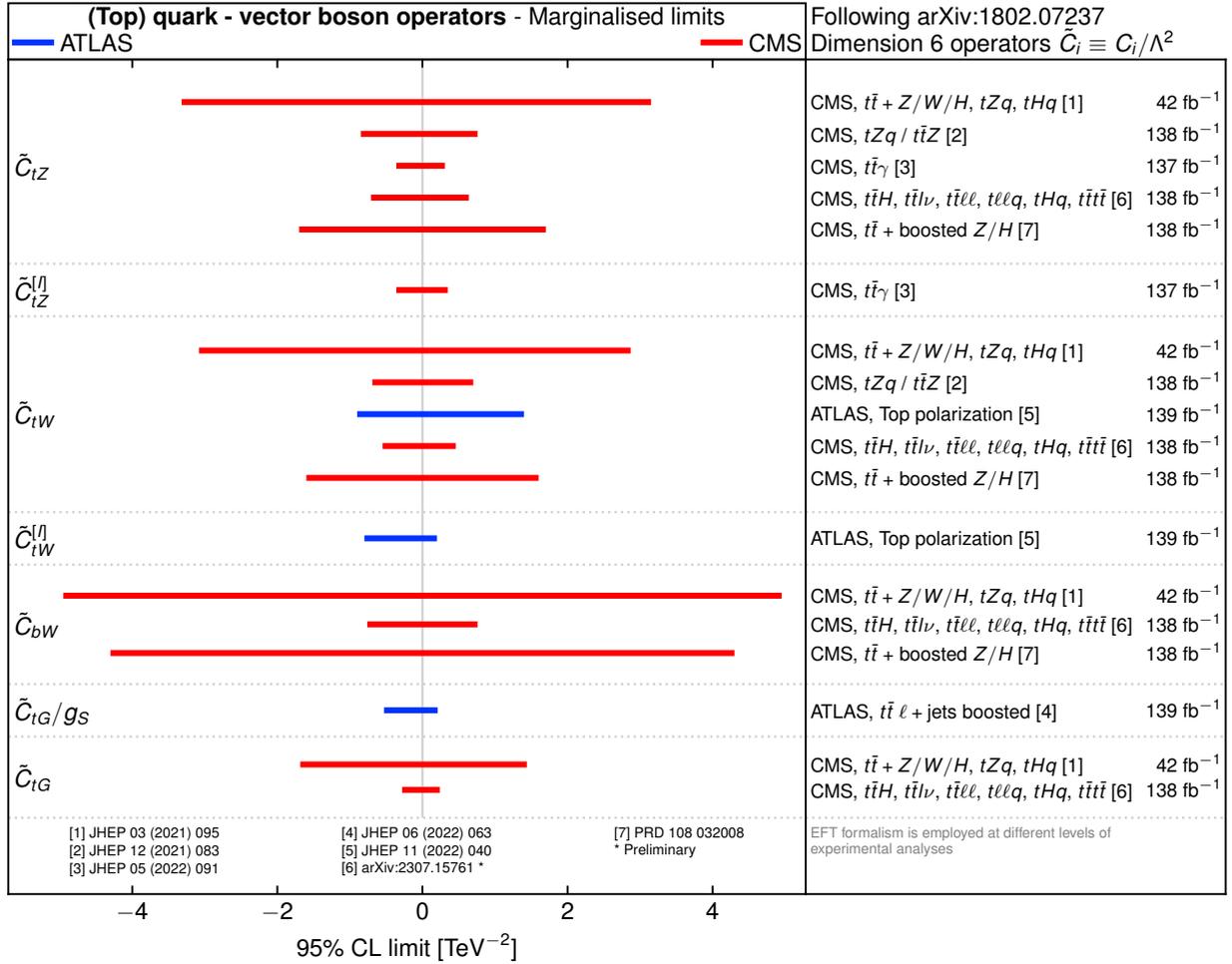
Figure 13: Summary of the 95% confidence level observed limits on the effective field theory Wilson coefficients of the dimension-6 operators related to (top) quark interaction with vector bosons, as obtained by the ATLAS and CMS Collaborations. The results are reported as marginalised constraints, treating all Wilson coefficients contributing to a given process as free parameters. The effect of a given Wilson coefficient is considered in multiple processes, where indicated in the references, and across multiple bins of differential measurements. Each row presents all the marginalised constraints obtained from a single fit. Vertical format.
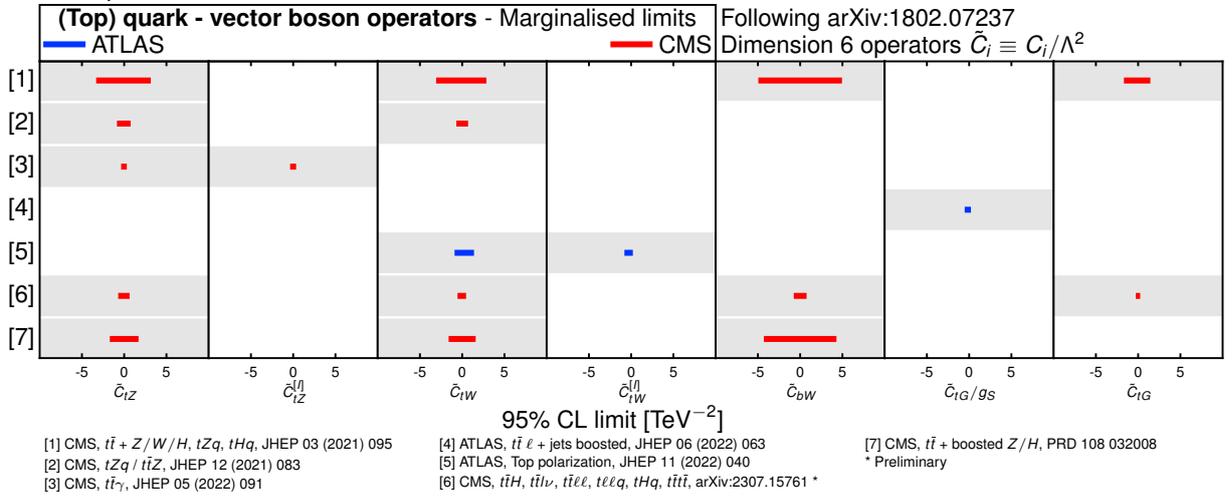
Figure 14: Summary of the 95% confidence level observed limits on the effective field theory Wilson coefficients of the dimension-6 operators related to (top) quark interaction with vector bosons, as obtained by the ATLAS and CMS Collaborations. The results are reported as marginalised constraints, treating all Wilson coefficients contributing to a given process as free parameters. The effect of a given Wilson coefficient is considered in multiple processes, where indicated in the references, and across multiple bins of differential measurements. Each row presents all the marginalised constraints obtained from a single fit. Horizontal format.
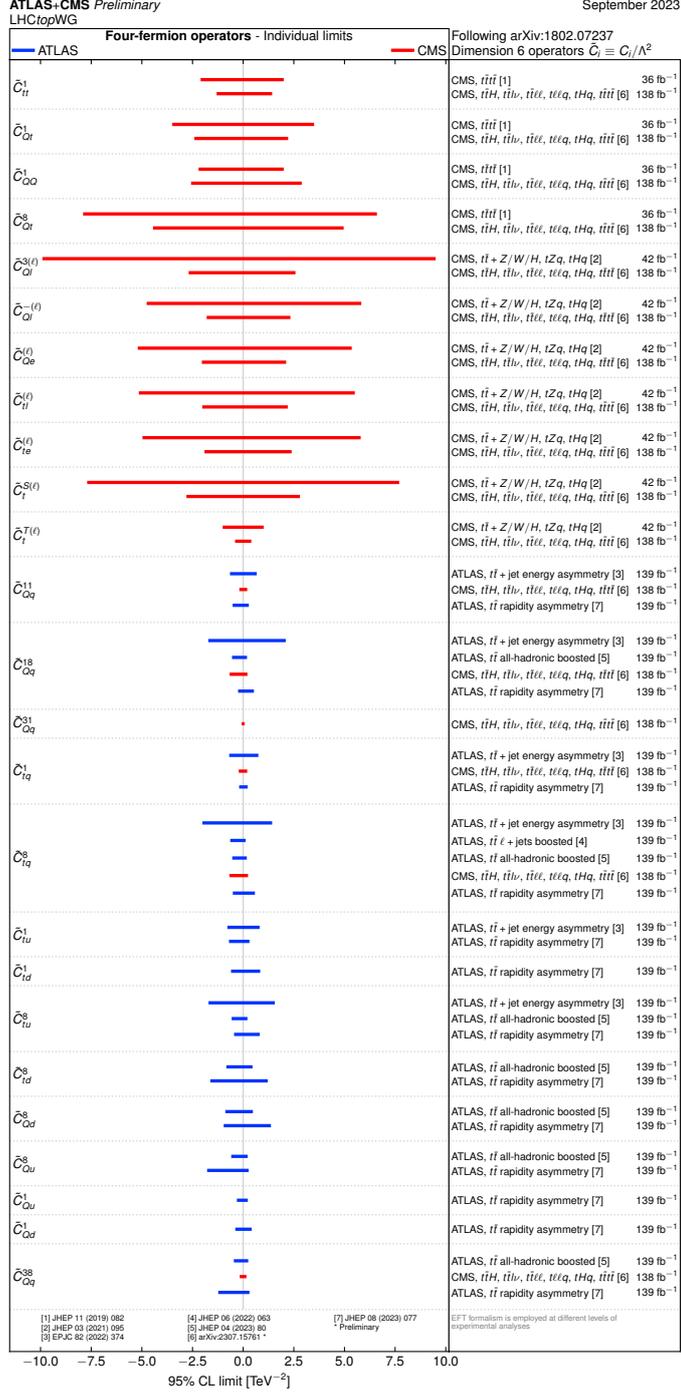
Figure 15: Summary of the 95% confidence level observed limits on the effective field theory Wilson coefficients of the dimension-6 operators related to four-fermion interactions, as obtained by the ATLAS and CMS Collaborations. The results are reported as individual constraints assuming new physics contributions from one specific operator at a time. Interpretations use the SMEFT framework and the Warsaw basis. The formalism is employed at different levels of the experimental analyses, from the interpretation of measured observables to a comparison of the data to simulations at the detector level. Most interpretations follow the LHCtopWG recommendations from arXiv:1802.07237. Vertical format.

Figure 16: Summary of the 95% confidence level observed limits on the effective field theory Wilson coefficients of the dimension-6 operators related to four-fermion interactions, as obtained by the ATLAS and CMS Collaborations. The results are reported as individual constraints assuming new physics contributions from one specific operator at a time. Interpretations use the SMEFT framework and the Warsaw basis. The formalism is employed at different levels of the experimental analyses, from the interpretation of measured observables to a comparison of the data to simulations at the detector level. Most interpretations follow the LHCtopWG recommendations from arXiv:1802.07237. Horizontal format.
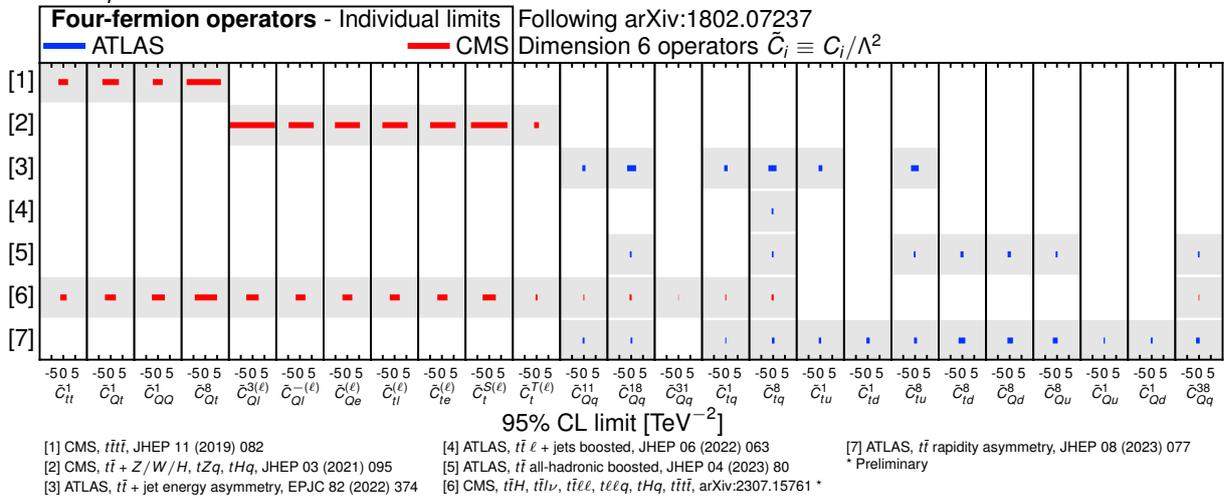
Figure 17: Summary of the 95% confidence level observed limits on the effective field theory Wilson coefficients of the dimension-6 operators related to four-fermion interactions, as obtained by the ATLAS and CMS Collaborations. The results are reported as marginalised constraints, treating all Wilson coefficients contributing to a given process as free parameters. The effect of a given Wilson coefficient is considered in multiple processes, where indicated in the references, and across multiple bins of differential measurements. Each row presents all the marginalised constraints obtained from a single fit. Vertical format.
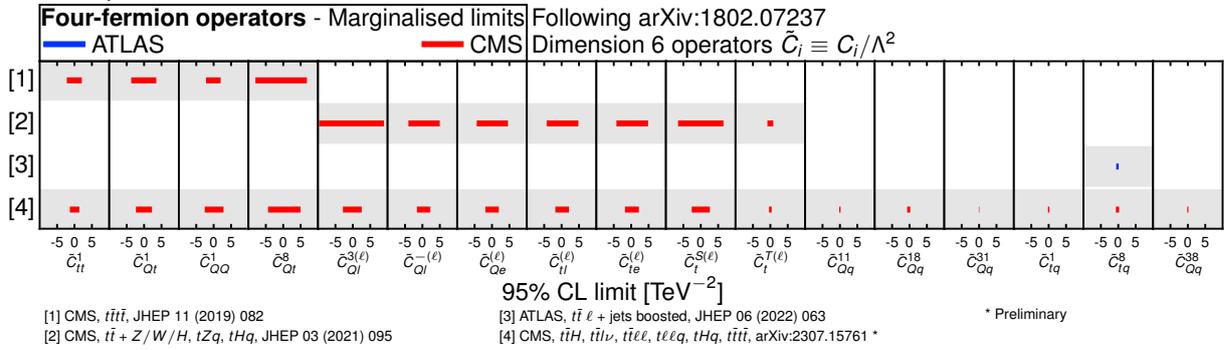
Figure 18: Summary of the 95% confidence level observed limits on the effective field theory Wilson coefficients of the dimension-6 operators related to four-fermion interactions, as obtained by the ATLAS and CMS Collaborations. The results are reported as marginalised constraints, treating all Wilson coefficients contributing to a given process as free parameters. The effect of a given Wilson coefficient is considered in multiple processes, where indicated in the references, and across multiple bins of differential measurements. Each row presents all the marginalised constraints obtained from a single fit. Horizontal format.

References

[1] W. Buchmuller and D. Wyler,
     Effective Lagrangian Analysis of New Interactions and Flavor Conservation,
     Nucl. Phys. B **268** (1986) 621 (cit. on p. 2).

[2] B. Grzadkowski, M. Iskrzynski, M. Misiak and J. Rosiek,
     Dimension-Six Terms in the Standard Model Lagrangian, JHEP **10** (2010) 085,
     arXiv: 1008.4884 [hep-ph] (cit. on p. 2).

[3] D. Barducci et al.,
     Interpreting top-quark LHC measurements in the standard-model effective field theory,
     (2018), ed. by J. A. Aguilar-Saavedra et al., arXiv: 1802.07237 [hep-ph] (cit. on p. 2).

[4] ATLAS Collaboration,
     Measurement of the polarisation of single top quarks and antiquarks produced in the t-channel at
     $\sqrt{s}$ *= 13 TeV and bounds on the tWb dipole operator from the ATLAS experiment*,
     JHEP **11** (2022) 040, arXiv: 2202.11382 [hep-ex] (cit. on pp. 2–5).

[5] ATLAS Collaboration, *Measurement of the $t\bar{t}Z$ and $t\bar{t}W$ cross sections in proton-proton collisions*
     at $\sqrt{s}$ = 13 TeV with the ATLAS detector, Phys. Rev. D **99** (2019) 072009,
     arXiv: 1901.03584 [hep-ex] (cit. on pp. 2–4).

[6] ATLAS Collaboration, *Measurements of differential cross-sections in top-quark pair events with a*
     high transverse momentum top quark and limits on beyond the Standard Model contributions to
     top-quark pair production with the ATLAS detector at $\sqrt{s}$ = 13 TeV, JHEP **06** (2022) 063,
     arXiv: 2202.12134 [hep-ex] (cit. on pp. 2–5).

[7] ATLAS Collaboration,
     Evidence for the charge asymmetry in pp $\rightarrow$ $t\bar{t}$ production at $\sqrt{s}$ = 13 TeV with the ATLAS detector,
     JHEP **08** (2023) 077, arXiv: 2208.12095 [hep-ex] (cit. on pp. 2, 3, 5, 8).

[8] ATLAS Collaboration, *Differential $t\bar{t}$ cross-section measurements using boosted top quarks in the*
     all-hadronic final state with 139 fb^{-1} of ATLAS data, JHEP **04** (2023) 080,
     arXiv: 2205.02817 [hep-ex] (cit. on pp. 2, 3, 5).

[9] ATLAS Collaboration, *Measurement of the energy asymmetry in $t\bar{t}j$ production at* 13 *TeV with the*
     ATLAS experiment and interpretation in the SMEFT framework, Eur. Phys. J. C **82** (2022) 374,
     arXiv: 2110.05453 [hep-ex] (cit. on pp. 2, 3, 5).

[10] ATLAS Collaboration, *Search for flavor-changing neutral-current couplings between the top quark*
     and the Z boson with proton-proton collisions at s=13 TeV with the ATLAS detector,
     Phys. Rev. D **108** (2023) 032019, arXiv: 2301.11605 [hep-ex] (cit. on pp. 3, 4).

[11] ATLAS Collaboration,
     Search for flavour-changing neutral current interactions of the top quark and the Higgs boson in
     events with a pair of τ-leptons in pp collisions at $\sqrt{s}$ = 13 TeV with the ATLAS detector,
     JHEP **2306** (2023) 155, arXiv: 2208.11415 [hep-ex] (cit. on pp. 3, 4).

[12] ATLAS Collaboration, *Search for flavour-changing neutral-current interactions of a top quark and*
     a gluon in pp collisions at $\sqrt{s}$ = 13 TeV with the ATLAS detector, Eur. Phys. J. C **82** (2022) 334,
     arXiv: 2112.01302 [hep-ex] (cit. on pp. 3, 4).

[13] ATLAS Collaboration, *Search for flavour-changing neutral-current couplings between the top quark and the photon with the ATLAS detector at s=13 TeV*, Phys. Lett. B **842** (2023) 137379, arXiv: 2205.02537 [hep-ex] (cit. on pp. 3, 4).

[14] CMS Collaboration, *Measurements of $t\bar{t}$ differential cross sections in proton-proton collisions at $\sqrt{s}$ = 13 TeV using events containing two leptons*, JHEP **02** (2019) 149, arXiv: 1811.06625 [hep-ex] (cit. on pp. 3, 4).

[15] CMS Collaboration, *Measurement of the top quark polarization and $t\bar{t}$ spin correlations using dilepton final states in proton-proton collisions at $\sqrt{s}$ = 13 TeV*, Phys. Rev. D **100** (2019) 072002, arXiv: 1907.03729 [hep-ex] (cit. on pp. 3, 4).

[16] CMS Collaboration, *Search for the production of four top quarks in the single-lepton and opposite-sign dilepton final states in proton-proton collisions at $\sqrt{s}$ = 13 TeV*, JHEP **11** (2019) 082, arXiv: 1906.02805 [hep-ex] (cit. on pp. 3, 5).

[17] CMS Collaboration, *Search for new physics in top quark production in dilepton final states in proton-proton collisions at $\sqrt{s}$ = 13 TeV*, Eur. Phys. J. C **79** (2019) 886, arXiv: 1903.11144 [hep-ex] (cit. on pp. 3, 4).

[18] CMS Collaboration, *Measurement of top quark pair production in association with a Z boson in proton-proton collisions at $\sqrt{s}$ = 13 TeV*, JHEP **03** (2020) 056, arXiv: 1907.11270 [hep-ex] (cit. on pp. 3, 4).

[19] ATLAS and CMS Collaborations, *Combination of the W boson polarization measurements in top quark decays using ATLAS and CMS data at $\sqrt{s}$ = 8 TeV*, JHEP **08** (2020) 051, arXiv: 2005.03799 [hep-ex] (cit. on pp. 3, 4).

[20] CMS Collaboration, *Search for new physics in top quark production with additional leptons in proton-proton collisions at $\sqrt{s}$ = 13 TeV using effective field theory*, JHEP **03** (2021) 095, arXiv: 2012.04120 [hep-ex] (cit. on pp. 3–5).

[21] CMS Collaboration, *Probing effective field theory operators in the associated production of top quarks with a Z boson in multilepton final states at $\sqrt{s}$ = 13 TeV*, JHEP **12** (2021) 083, arXiv: 2107.13896 [hep-ex] (cit. on pp. 3–5).

[22] CMS Collaboration, *Measurement of the inclusive and differential $t\bar{t}\gamma$ cross sections in the dilepton channel and effective field theory interpretation in proton-proton collisions at $\sqrt{s}$ =13 TeV*, JHEP **05** (2022) 091, arXiv: 2201.07301 [hep-ex] (cit. on pp. 3–5).

[23] CMS Collaboration, *Search for new physics using effective field theory in 13 TeV pp collision events that contain a top quark pair and a boosted Z or Higgs boson*, Phys. Rev. D **108** (2023) 032008, arXiv: 2208.12837 [hep-ex] (cit. on pp. 3–5).

[24] CMS Collaboration, *Search for physics beyond the standard model in top quark production with additional leptons in the context of effective field theory*, (2023), arXiv: 2307.15761 [hep-ex] (cit. on pp. 3–6).